Protein Science (1998), 7:2136–2142. Cambridge University Press. Printed in the USA.

Tertiary structure-dependence of misfolding substitutions in loops of the maltose-binding protein

SÉBASTIEN RAFFY, NATHALIE SASSOON, MAURICE HOFNUNG, AND JEAN-MICHEL BETTON

Unité de Programmation Moléculaire et de Toxicologie Génétique/CNRS-URA1444, Département des Biotechnologies, Institut Pasteur, 25 rue du Docteur Roux, Paris 75015, France

(RECEIVED May 11, 1998; ACCEPTED June 19, 1998)

Abstract

We previously identified and characterized amino acid substitutions in a loop connecting helix I to strand B, the αI/βB loop, of the N-domain that are critical for in vivo folding of the maltose-binding protein (MalE31). The tertiary context-dependence of this mutation in MalE folding was assessed by probing the tolerance of an equivalent $\alpha\beta$ loop of the C-domain to the same amino acid substitutions (MalE219). Moving the loop mutation from the N- to the C-domain eliminated the in vivo misfolding step that led to the formation of inclusion bodies. In vitro, both loop variants exhibited an important decrease of stability, but their intrinsic tendency to aggregate was well correlated with their periplasmic fates in *Escherichia coli*. Furthermore, the noncoincidence of the unfolding and refolding transition curves and increase of light scattering during the refolding of MalE31 indicate that a competing off-pathway reaction could occurs on the folding pathway of this variant. These results strongly support the notion that the formation of super-secondary structures of the N-domain is a rate-limiting step in the folding pathway of MalE.

Keywords: $\alpha\beta$ loop; inclusion bodies; maltose-binding protein; protein folding

The most widely used and best studied host for high-level production of recombinant proteins is *Escherichia coli*. However, many of these proteins are produced in the form of biologically inactive and aggregated forms or inclusion bodies. The conventional molecular mechanism of this process suggests that in vivo folding intermediates are responsible for the formation of these aggregates, and that folding and aggregation are competing processes (Mitraki & King, 1989). According to this model, amino acid substitutions play an active role in directing the polypeptide chain along a nonproductive folding pathway (Wetzel, 1994).

Maltose-binding protein (MalE or MBP) functions in the periplasm of *E. coli* where it serves as a soluble receptor for the high affinity transport of maltose and maltodextrins (Nikaido, 1994). Because of its key role in maltose transport, productive export and folding of MalE in the periplasm is essential for cells to utilize maltose as a carbon source. This feature facilitated the use of genetic selections and screens for analyzing MalE export and folding. MalE is synthesized in the cytoplasm as a precursor protein, preMalE, with an amino-terminal signal sequence that serves to target the precursor protein to the translocation machinery (Wickner & Leonard, 1996). After translocation across the cytoplasmic membrane, the signal sequence is cleaved off by the signal peptidase, the mature MalE protein is released from the membrane into the periplasm and folds to its native structure. High-resolution three-dimensional structure of both the nonliganded and maltose-bound forms of MalE have been reported (Spurlino et al., 1991; Sharff et al., 1992). The overall structure of MalE consists of two discontinuous domains surrounding a cleft that forms the binding site for maltose and maltodextrins. The two domains, designated as the N- and C-domains, are constructed from secondary structural $\beta\alpha\beta$ units.

One approach to identify amino acid residues that are critical in the folding pathway of a protein is to generate mutations by random mutagenesis and screen for a phenotype based on folding alterations. In earlier work, by using maltose phenotypes, we identified misfolding amino acid substitutions in a loop connecting the α-helix I to β-strand B of the N-domain of MalE (Betton et al., 1996). Among these mutations, the most defective variant, MalE31, corresponded to the double substitution of the wild-type Gly32–Ile33 by an Asp32–Pro33 sequence. In vivo, the preMalE31 was efficiently exported and processed, but the defective folding of the mature protein led to the formation of inclusion bodies in the periplasm (Betton & Hofnung, 1996). One major physiological consequence for the cells overproducing MalE31 was an induction of a heat-shock response regulated by the alternate heat-shock σ^E factor (Missiakas et al., 1996). However, MalE31 could be purified from inclusion bodies, after a urea-solubilization step, and in vitro the renatured variant exhibited complete maltose-binding activity. Thus, the modified $\alpha\beta$ loop, which is distant from the binding site,

Reprint requests to: Jean-Michel Betton, Unité de Programmation Moléculaire et de Toxicologie Génétique, CNRS-URA 1444, Département des Biotechnologies, Institut Pasteur, 25 Rue du Docteur Roux, Paris 75015, France; e-mail: jmbetton@pasteur.fr.

did not perturb the function but rather the periplasmic folding of MalE.

In this study, we assess the tertiary structure-dependence of the MalE31 amino acid substitution by replacing the same mutation in an equivalent loop connecting the α-helix VII to β-strand J of the C-domain. The new loop variant, MalE219, displays a productive periplasmic folding pathway and a biologically active structure. We further report the in vitro analysis of the refolding of this variant compared with the MalE31 and wild-type proteins. These results confirm that formation of the supersecondary structure of the N-domain, to which belongs the modified loop of MalE31, is crucial for the productive folding pathway of MalE.

Results

The $\alpha\beta$ connections of MalE

In designing equivalent MalE31 amino acid substitutions (same Asp-Pro substitution in a similar secondary context) in a different tertiary context, it seemed important to conserve the $\alpha\beta$ loop characteristics as possible. There are four $\alpha\beta$ loops in the MalE structure: two in the N-domain and two in the C-domain. In the $\alpha\beta$1 loop, the transition from helix to strand is mainly achieved by one Gly residue with a positive value of the ϕ angle, which changes the direction of the polypeptide chain (Edwards et al., 1987). In this regard, the $\alpha\beta$ loop connecting the α-helix VII to β-strand J in the C-domain was found to be the best candidate. Furthermore, structural comparison of the four $\alpha\beta$ loops, investigated by superimposing α-carbon backbones, confirmed that among these structural connections, the αVII-βJ loop of the C-domain was structurally the closest loop to the αI/βB loop (the lowest root-mean-square deviation to the αI/βB template, data not shown). To study the tolerance of MalE31 substitution in this new structural environment, Gly220 and Glu221 were simultaneously substituted by Asp and Pro. The resulting MalE variant was designated MalE219 because this number corresponds to the N-terminus flanking position of the modified site (the same nomenclature was used for MalE31). A common feature of most parallel α/β proteins is that active sites are always located in the C-termini of the β strands. Therefore, from their location in the three-dimensional structure of MalE (Fig. 1), both modified loops are distant from the maltose-binding cleft.

In vivo properties of loop mutants

Previous studies have shown that the Mal$^-$ phenotype of cells expressing *malE31* was due to the defective folding of the corresponding mature protein that forms inclusion bodies in the periplasm (Betton & Hofnung, 1996). In contrast, cells expressing *malE219* (from plasmid p219H) were able to complement the chromosomal nonpolar deletion Δ*malE444* for maltose fermentation on MacConkey maltose plates and supported growth on maltose minimal medium (Table 1). This mutant (p219H) displayed only a slightly lower rate of maltose uptake than the wild-type (p1H). Because *malE219* is correctly expressed at a level comparable to the *malE* gene (Table 1; Fig. 2), the physiological characteristics of cells expressing this mutant (maltose phenotypes and maltose uptake rates) are in excellent agreement with a productive periplasmic folding pathway and a biologically active structure of the corresponding mature MalE219 protein.

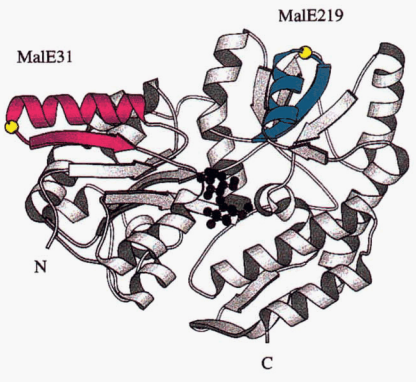

Fig. 1. $\alpha\beta$ loop variants. Location of modified loops in the tertiary structure of MalE. Helix 1 and strand βB are colored in purple, helix VII and strand βJ in blue, respectively, and bound maltos in black. For both loops, the Gly residue with a positive value of the ϕ angle is shown in yellow. The drawing was generated with Molscript (Kraulis, 1991).

Periplasm/membrane fractionation

The formation of inclusion bodies can be biochemically determined by soluble/insoluble separation based on fractionation by centrifugation of native lysates (Haase-Pettingell & King, 1988). Figure 3 shows that MalE31 is found in the pellet as expected for inclusion bodies. In contrast, MalE219 is found exclusively in the soluble fraction (periplasmic fraction). Although the correct cellular location of MalE219 in cells producing this variant is well correlated with their ability to grow on maltose minimal medium, its periplasmic level was lower than wild-type MalE (Table 1; Fig. 3). This result suggests that MalE219 is correctly synthesized and exported but partially degraded in the periplasm. To understand the relative contributions of the properties of the host cell (expression system) and the properties of the protein, to the periplasmic fate of a newly translocated protein, we purified MalE31 and MalE219 and investigated their intrinsic folding properties.

Equilibrium folding studies

In vitro, as indicated in Table 2, the three proteins exhibited similar maltose binding affinity. Thus, the purified MalE31 and MalE219 proteins appear to be properly folded to a native structure. The Gdn–HCl-induced unfolding and refolding transitions of variants were followed by tryptophan fluorescence that monitors the overall tertiary structure of MalE (Fig. 4). MalE31 and MalE219 have clearly decreased stabilities (Table 2, C_m values). However, the unfolding and refolding transition curves observed for MalE31 did not coincide. Indeed, both transition curves are separated by a significant midpoint difference (0.4 M Gdn–HCl). Incubation of the samples for longer times (for up to 24 h in the denaturation step and for up to 72 h in the renaturation step) at two different protein concentrations (80 and 8 μg/mL) yields almost identical transition curves (data not shown), implying that there is no slow protein concentration-dependent equilibrium. Further control experiments carried out with MalE31 purified by maltose-free ion exchange chromatography indicated that this apparent hysteresis was not due to the presence of residual maltose. From the phenomenon shown in Figure 4, it is clear that Gdn–HCl-induced denaturation of MalE31 does not proceed via a two-state model, but instead some kinetic barrier and off-pathway reactions must exist. This particular be-

Table 1. *Properties of the malE mutants*

Plasmid[a]	Phenotype maltose[b]	DT (min)[c]	Maltose uptake[d] (pmol/min/10^9 cells)	Expression[e] (%)	Periplasmic yield[f] (μg/mg)
p1H	++	215 ± 20	5.5 ± 0.5	100	35 ± 2
p31H	−	500 ± 30	0.15 ± 0.05	86	0.15 ± 0.01
p219H	+	260 ± 25	4.0 ± 0.2	77	20 ± 2
pΔ709	−	535 ± 40	0.05 ± 0.05	0	0

[a]Plasmids p1H, p31H, and p219 H encode MalE, MalE31, and MalE219, respectively. pΔ709 is a negative control.
[b]Symbols indicate maltose utilization assayed on MacConkey plates after overnight incubation at 37 °C.
[c]Doubling time in synthetic liquid M63B1 maltose medium at 37 °C assessed by following the turbidity at 600 nm.
[d]Initial rates of maltose uptake measured at 1.5 μM maltose.
[e]Immunoblot shown in Figure 2 was scanned and relative steady-state levels of MalE were normalized to EF-Tu.
[f]Steady-state levels of MalE in periplasmic fractions assessed by a sandwich immunoassay and normalized to protein content of whole cells determined by the Bradford procedure using bovine serum albumin as a standard.

havior of MalE31, in the absence of cellular factors, is consistent with its tendency to form inclusion bodies in vivo.

Unfolding and refolding kinetics

The kinetics of unfolding in the presence of 1.4 M Gdn–HCl (a denaturant concentration at which the three proteins are fully unfolded as depicted in Fig. 4) were measured by the decrease in tryptophan fluorescence (Fig. 5A). For all three proteins the unfolding process is described by a single phase that accounts for 100% of the difference expected between native and denatured proteins. The major difference was observed for the unfolding rate of MalE219, which is found threefold faster than for the wild-type and MalE31 proteins. This result is in agreement with the strong destabilization effect of that mutation, as previously observed from the equilibrium measurements.

The refolding process of the wild-type and variant proteins, after denaturation in 4 M and renaturation in 0.06 M Gdn–HCl (a denaturant concentration at which the three proteins are fully folded), appeared to be at least triphasic (Fig. 5B). The first phase was too fast to be analyzed by manual mixing (dead time of 10 s). However, this phase was detected because its amplitude accounted for approximately 25% of the signal recorded between native and denatured proteins. The remaining change in fluorescence accompanying refolding (75%) decomposed in two phases: a faster phase (30%) and a slower phase (45%). Both loop variants displayed a decrease in refolding rate and change in amplitude of the detected refolding phases. The final refolding yield of the MalE variants, reported in Table 3, reflected their intrinsic tendency to misfold.

In vitro aggregation

To study in vitro the aggregation of folding intermediates, we measured classical light scattering during the refolding kinetics of MalE variants. Previous refolding studies, carried out with a low MalE31 concentration (5 μg/mL) and at 25 °C, failed to detect significant light scattering during this process. Generally, the extent of aggregation is greater at higher temperature and protein concentrations due to the strong temperature- and concentration-dependence of the multimolecular, hydrophobic interactions that determine these reactions. Hence, light scattering was measured at

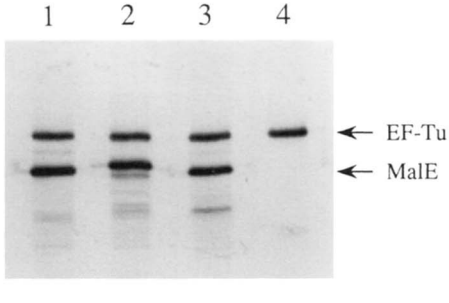

Fig. 2. Production of loop variants. Whole-cell extracts from experiment shown in Figure 3 (10-fold diluted samples) were separated by SDS-polyacrylamide gel electrophoresis. Immunoblot analysis of the gel was performed by using a mixure of rabbit antibodies directed against MalE and against EF-Tu. Lanes: (1) p1H, (2) p31H, (3) p219H, and (4) pΔ709. Densitometric analysis of the MalE band was normalized to the level of the EF-Tu band.

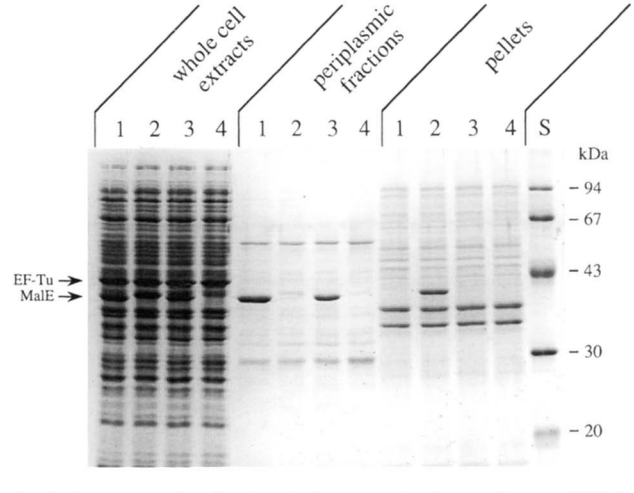

Fig. 3. Subcellular localization. Cells, grown in rich medium at 30 °C for 3 h, were fractionated from spheroplasts. Soluble (periplasm) and insoluble fractions (pellets), corresponding to 10^8 bacteria, were separated by SDS-polyacrylamide gel electrophoresis (12.5% acrylamide). The gel was stained with Coomassie blue. Lanes: (1) p1H, (2) p31H, (3) p219H, and (4) pΔ709.

Table 2. *Maltose binding and folding properties of the purified MalE variants*

Protein	Maltose binding (K_d)[a] (μM)	C_m (M)	m[d] (kcal/mol^2)	ΔG_{H_2O} (kcal/mol)
MalE-wt	1.8 ± 0.5	1.05 ± 0.05	9 ± 2	−10 ± 1
MalE31	1.5 ± 0.5	0.75 ± 0.05[c] 0.35 ± 0.05[d]	—	Not determined
MalE219	2.5 ± 0.5	0.35 ± 0.01	9 ± 2	−3.5 ± 0.5

[a]Dissociation constant for maltose-binding measured by fluorescence titration at 345 nm (excitation: 295 nm).
[b]Dependence of the free energy difference on Gdn–HCl concentration.
[c]Gdn–HCl concentration at the midpoint of the unfolding transition of MalE31.
[d]Gdn–HCl concentration at the midpoint of the refolding transition of MalE31.

30 °C and 80 μg/mL protein concentration. Under these conditions, the intensity of light scattered by MalE31 increased with refolding time. When MalE219 and wild-type protein were examined by this technique, under the same experimental conditions, no increase was observed, but rather a slight decrease. Because productive renaturation was minimal under the conditions chosen, the light scattering was mainly due to the multimeric aggregates of MalE31 in solution. Once again, this result is consistent with inclusion body formation during the periplasmic folding of MalE31. Although the progress curve, shown in Figure 6, was fitted by two exponential terms, none was found to correspond to those found for the refolding phases assessed by fluorescence.

Discussion

To investigate the tertiary structure-dependence of the misfolding and destabilizing mutation of MalE31, the same double substitution was constructed in an equivalent secondary structural context, $\alpha\beta 1$ loop, of the C-domain. In contrast to MalE31, the results presented here clearly demonstrate that MalE219 was correctly folded and functionally active in the periplasm of *E. coli*. Thus, the local tertiary environment of the C-domain might allow the substituted residues to form a native loop conformation in the structure of folding intermediates along the productive folding pathway.

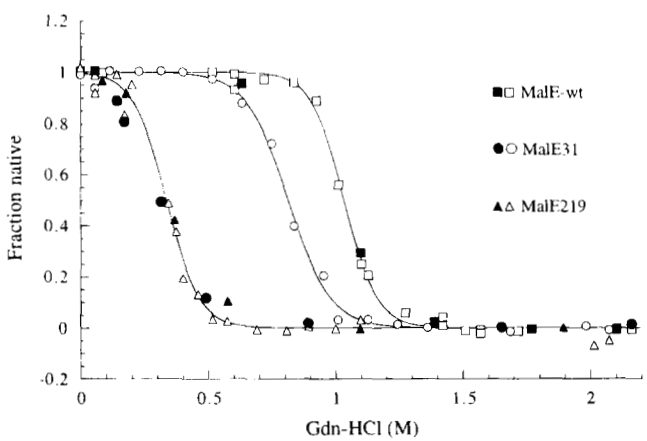

Fig. 4. Unfolding–refolding equilibrium transitions. The Gdn–HCl-induced transitions were assessed by the fluorescence emission at 345 nm (excitation wavelength: 295 nm). Open symbols are for the denaturation process and the filled symbols for the renaturation process. The experimental curves were normalized by using the relation $f_N = (Y - Y_D)/(Y_N - Y_D)$, where Y_N and Y_D are the fluorescence of the native and unfolded MalE, respectively, and f_N is the fraction of native protein.

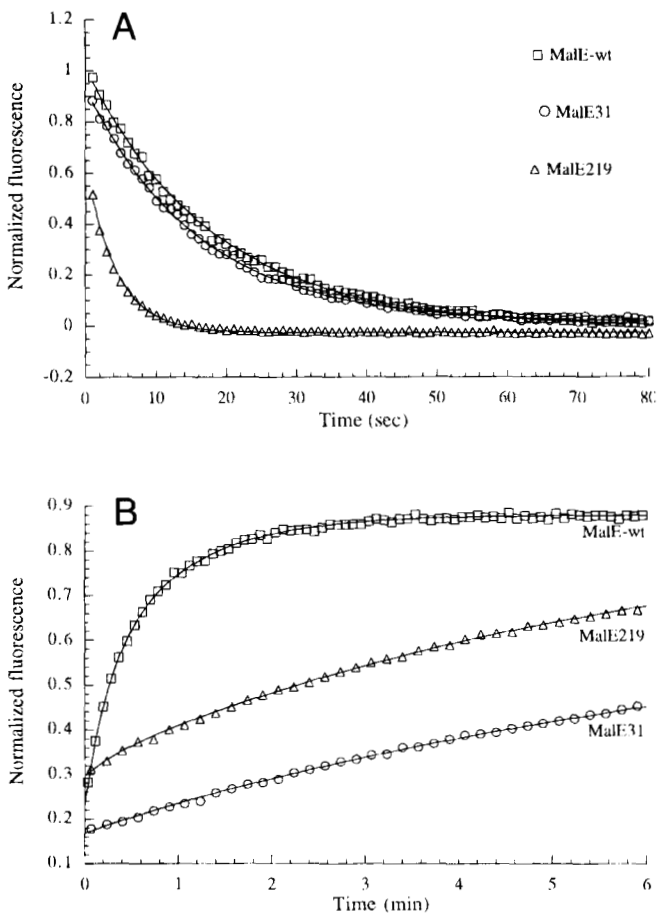

Fig. 5. Unfolding and refolding kinetics. Kinetics were monitored by tryptophan fluorescence at 345 nm, excitation at 295 nm. **A:** Unfolding was initiated by mixing native proteins (0.5 mg/mL) in 1.4 M Gdn–HCl, 50 mM HEPES buffer, pH 7.5 at 25 °C. **B:** Refolding was initiated by mixing previously unfolded proteins (0.5 mg/mL) in 4.2 M Gdn–HCl with 70 volumes of 50 mM HEPES buffer, pH 7.5 at 25 °C. Fluorescence intensities of the unfolded proteins in 4.2 M Gdn–HCl and native proteins were taken as 0 and 100%, respectively. The solid lines are best fits of the data to single (unfolding) or double (refolding) exponential terms.

Table 3. *Kinetic parameters for the denaturation and renaturation of MalE variants*

Protein	Unfolding relaxation time[a] (s)	Refolding relaxation time[b] (s)	Refolding relative amplitude[c] (%)	Refolding yield[d] (%)
MalE-wt	16 ± 2	τ_f = 15 ± 1 τ_s = 60 ± 6	A_f = 30 ± 2 A_s = 43 ± 2	88 ± 2
MalE31	17 ± 2	τ_f = 110 ± 10 τ_s = 600 ± 50	A_f = 3 ± 0.5 A_s = 75 ± 5	70 ± 2
MalE219	4 ± 0.1	τ_f = 17 ± 2 τ_s = 400 ± 25	A_f = 3 ± 0.5 A_s = 65 ± 5	88 ± 2

[a]Relaxation time of unfolding kinetics, at 25 °C, in 1.4 M Gdn–HCl.
[b]Relaxation time of fast (τ_f) and slow (τ_s) phases of refolding kinetics in 0.06 M Gdn–HCl.
[c]Relative amplitudes of fast (A_f) and slow (A_s) recorded phases of the same refolding kinetics.
[d]Total amplitude of the refolding kinetics, at 25 °C, in 0.06 M Gdn–HCl.

Although previous mutational analysis of amino acid substitutions at positions 32 and 33 identified several defective folding variants with non-Pro substitutions, the dramatic mutational effect in the aggregation of MalE31 could be attributed to the proline substitution. Since the hypothesis of Brandts (Brandts et al., 1975) that *cis-trans* isomerization of peptidyl-Pro bonds can be associated with rate-limiting folding steps, this isomerization is now established as a slow reaction in the folding of many proteins (Nall, 1994). Because both loop variants (MalE31 and MalE219) refold more slowly than MalE-wt, it is likely that slow refolding phases of these variants involved proline *cis-trans* isomerization. However, in performing double jump experiments, we never detected a slow equilibrium between slow unfolded forms of MalE31 (Betton & Hofnung, 1996). Alternatively, slow refolding phases could be accounted for by fast isomerization steps forming early misfolded species or by slow proline isomerization in a folded state (Nall, 1994). Nevertheless, it is clear that Pro33 drastically alter the folding pathway of MalE, presumably by allowing an alternative misfolded structure to form. The distribution of protein species during folding could be determined by changes in the activation energy barriers between intermediates "on" or "off" in the folding pathway (Baker & Agard, 1994). Interestingly, a striking hysteresis was only observed with MalE31, and not with MalE219. This phenomenon strongly suggests that misfolded states are kinetically trapped during the renaturation process, and corroborates the model previously proposed for the periplasmic folding of MalE31 (Betton et al., 1998). Such a kinetic partitioning has been shown to occur in the denaturant-induced transitions of bacterial luciferase (Sinclair et al., 1994), bovine carbonic anhydrase (Cleland & Wang, 1990), egg white lysosyme (Goldberg et al., 1991), horse muscle phosphoglycerate kinase (Mitraki et al., 1987), and P22 tailspike protein (Speed et al., 1995).

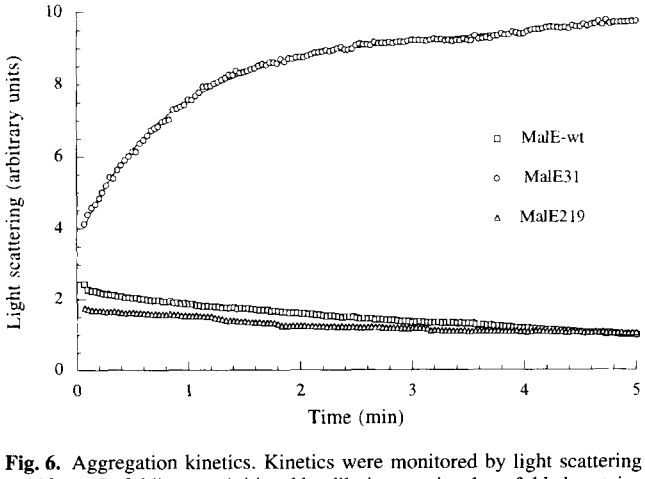

Fig. 6. Aggregation kinetics. Kinetics were monitored by light scattering at 320 nm. Refolding was initiated by diluting previously unfolded proteins (2.5 mg/mL) in 4.2 M Gdn–HCl with 30 volumes of 50 mM HEPES buffer, pH 7.5 at 30 °C. The solid line is the best fit of the data to a double exponential term.

The ability of the modified sequence to successfully substitute for a particular loop depends not only on the intrinsic characteristics of the amino acid residues, but also on the structural environment within the protein. In this regard, the formation of αVII-βJ supersecondary structure of the C-domain is more tolerant to amino acid modifications than the αI-βB structure. It should be noted that the substitutions are located away from the maltose-binding site, in solvent-exposed regions. Examination of the three-dimensional structure of MalE reveals that within loop conformations, Gly32 and Gly220 terminate the preceding αI and αVII helices by forming a five-turn hydrogen bond; Ile33 and Glu221 initiate the following βB and βJ strands without participating in the hydrogen-bonding network of the corresponding β-sheets. However, Ile33, contrary to Glu221, is buried and forms a hydrophobic cluster with other residues (Betton et al., 1996), and both helices (αI and αVII) exhibit different orientations about their specific axes, relative to the respective β-strands, βB and βJ. The two αβ loops, when extended to include more of the secondary structure elements flanking the loops, display an important difference with respect to the topology of the β-sheet in which they occurred. Indeed, βαβ units are of two types: (1) adjacent in which the two β-strands are hydrogen-bond paired and (2) nonadjacent in which the two β-strands, although in the same β-sheet, are separated by one or more β-strands. The modified loop of MalE31 is part of the unique adjacent βαβ unit of the MalE structure, whereas the modified loop of MalE219 occurs in a nonadjacent unit.

Among several common features, the first six elements of secondary structure that constitute a large part of the N-domain of periplasmic binding proteins, have the same topological arrange-

ments (Quiocho, 1991). Amino acid substitutions in the N-domain that alter the folding pathway of MalE were previously isolated by a genetic selection based on protein export (Cover et al., 1987). Indeed, intragenic suppressive mutations of export-defective signal peptides of MalE were located in this domain. Furthermore, by studying the unfolding-refolding transition of the corresponding MalE variants, Randall and co-workers (Chun et al., 1993) have suggested that the rate-limiting step, both in vivo and in vitro, of the MalE folding pathway could be the formation of this super-secondary structure in the N-domain. With the same genetic strategy, similar results were found with the ribose-binding protein, which is structurally close to MalE (Song & Park, 1995). These studies highlighted both the importance and the difficulty to bring separated segments of the polypeptide chain into proximity to form the hydrophobic core of the N-domain.

Several studies carried out on various proteins produced in *E. coli* supported a correlation of thermodynamic stability with the extent of inclusion body formation. The results described here suggest that instead of ΔG, refolding kinetic properties of newly synthesized protein would better reflect the steady-state distribution among alternative pathways. As we have shown here, a strongly destabilized protein (MalE219) can be produced at a high level in the periplasm, whereas a less destabilized variant (MalE31) accumulates into inclusion bodies. In other words, aggregation seems more determined by long-term persisting folding intermediates of the rate-limiting step that controls kinetic partitioning between productive folding and misfolding pathways.

The above results argue that the information directing the polypeptide chain to the aggregation pathway is not only determined by the amino acid sequence, but also by the tertiary structure. Further study of the mechanism of misfolding by mutational modification will help elucidate inclusion body formation that interferes with the production of proteins in *E. coli.*

Materials and methods

Bacterial strains and plasmids

E. coli K12 strains pop6590 and pop6499, which are both derivatives of MC4100 (Betton et al., 1998), were used as host strain for phenotype characterizations and protein production, respectively. Both strains carry the nonpolar deletion of the chromosomal *malE* gene, Δ*malE444* (Shuman, 1982), and pop6499 harbors the $malT^{c1}$ allele, which confers constitutive and high-level expression on the maltose operons (Debarbouille et al., 1978). Plasmids p1H and p31H are pBR322 derivatives harboring the bacteriophage f1 origin, and carry the wild-type *malE* and *malE31* genes (Betton et al., 1996), respectively, under the control of their own promoters; the MalT-dependent *malEp* promoter. Plasmid pΔ709 is a p1H derivative that carries a deletion of the ribosome binding site and the first 256 codons of the *malE* gene (Betton & Hofnung, 1994), and was used as a negative control.

Site-directed mutagenesis

The *malE219* allele was constructed by oligonucleotide mutagenesis with single-stranded p1H DNA containing uracil as the template for primer extension and ligation (Kunkel, 1985). The mutagenic oligonucleotide used for the double substitution of codons 220 and 221 was: 5′-GG TCA TCG CTG **TTG GAT CCT** TAT TAA AGG C-3′. Mutant DNAs were first screened by restriction analysis for the presence of a *Bam*HI site (bases in bold type) and further sequenced by the dideoxy method using the Sequenase kit purchased from USB-Amersham. The resulting plasmid was named p219H.

Maltose uptake and binding assay

The initial rate of maltose transport was estimated by measuring uptake of ^{14}C-maltose and the dissociation constant of maltose (K_D) was assessed by tryptophan fluorescence titration as described previously (Betton & Hofnung, 1996).

Cell fractionation

Cultures were grown in LB medium supplemented with 0.1 mg/mL carbenicillin at 30 °C for 3 h ($Abs_{600} \approx 1$). Cells from 10 mL of the culture ($5 \cdot 10^8$ cells/mL) were harvested by centrifugation and fractionated by spheroplast preparation as previously described (Betton & Hofnung, 1996). The periplasmic fractions and pellets were analyzed by SDS-polyacrylamide gel electrophoresis (12.5% acrylamide). Proteins were either visualized by Coomassie blue staining or transferred to nitro-cellulose membranes prior immunodetection by specific antibodies as described previously (Betton & Hofnung, 1994). For quantitative analyses, gels or membranes were scanned with a ImageMaster VDS camera (Pharmacia Biotech, Uppsala, Sweden).

Protein purification

Strain pop6499, producing either wild-type or variant (MalE31 or MalE219) MalE, was grown to A_{600} of 1.5, at 30 °C, in LB medium supplemented with 0.1 mg/mL carbenicillin. The wild-type MalE and MalE219 proteins were released by osmotic shock (Neu & Heppel, 1965). The MalE31 protein was renatured from inclusion bodies after a urea-solubilization step, as previously described (Betton & Hofnung, 1996). All three proteins were purified by affinity chromatography using a crosslinked amylose resin (Ferenci & Klotz, 1978) and were eluted by 10 mM maltose. Maltose was removed from the proteins by extensive dialysis, and protein concentrations were determined from the absorbance at 280 nm with an extinction coefficient of $\epsilon = 68{,}750\ M^{-1} \cdot cm^{-1}$.

Equilibrium experiments

Solutions of native MalE proteins were diluted (5 μg/mL final protein concentration) in 50 mM HEPES buffer, pH 7.5, containing various Gdn–HCl concentrations (refractometrically determined) and incubated 4 h at 25 °C before spectroscopic measurements. All fluorescence measurements were carried out with a Fluoromax spectrofluorometer (Spex). The fluorescence emission intensities were recorded at 345 nm, and the excitation wavelength was 295 nm, with a spectral band width of 2 nm. The experimental data were analyzed by using the model of linear dependence of ΔG upon Gdn–HCl concentration (Pace, 1986).

Unfolding and refolding kinetics

Unfolding kinetics were initiated by adding native proteins at zero time to a HEPES buffer solution containing Gdn–HCl (1.4 M final concentration) at 25 °C. For refolding kinetics, previously unfolded

proteins (0.4 mg/mL in 4.2 M Gdn–HCl) were diluted into HEPES buffer (6 μg/mL protein in 0.06 M Gdn–HCl, final concentration) at 25 °C. Experimental data were fitted using the nonlinear regression analysis program Kaleidagraph (Synergy Software, Reading, Pennsylvania; PCS Inc., Reading, Pennsylvania).

Light-scattering measurements

Unfolded MalE variants (4.2 M Gdn–HCl, 2.5 mg/mL protein) were diluted 30-fold in the HEPES buffer at 30 °C. All the solutions were filtered through a 0.22-μM filter just before use. The kinetics were recorded with the spectrofluorimeter as described above, and using the same wavelength (320 nm) as excitation and emission settings.

Acknowledgments

This research was supported by funds from the Institut Pasteur, the Centre National de la Recherche Scientifique, and the Mision Physique et Chimique du Vivant (NE95N88/0021). We thank Yves Mechulam for the generous gift of EF-Tu antibodies and Emmett Jonhson for carefully reading the manuscript.

References

Baker D, Agard DA. 1994. Kinetics versus thermodynamics in protein folding. *Biochemistry 33*:7505–7509.

Betton J-M, Boscus D, Missiakas D, Raina S, Hofnung M. 1996. Probing the structural role of an $\alpha\beta$ loop of maltose-binding protein by mutagenesis: Heat-shock induction by loop variants of the maltose-binding protein that form periplasmic inclusion bodies. *J Mol Biol 262*:140–150.

Betton J-M, Hofnung M. 1994. *In vivo* assembly of active maltose binding protein from independently exported protein fragments. *EMBO J 13*:1226–1234.

Betton J-M, Hofnung M. 1996. Folding of a mutant maltose binding protein of *E. coli* which forms inclusion bodies. *J Biol Chem 271*:8046–8052.

Betton J-M, Sassoon N, Hofnung M, Laurent M. 1998. Degradation versus aggregation of misfolded maltose-binding protein in the periplasm of *Escherichia coli*. *J Biol Chem 273*:8897–8902.

Brandts JF, Halvorson HR, Brennan M. 1975. Consideration of the possibility that the slow step in protein denaturation reactions is due to *cis-trans* isomerism of proline residues. *Biochemistry 14*:4953–4963.

Chun S-Y, Strobel S, Bassford PJ, Randall LL. 1993. Folding of maltose-binding protein. *J Biol Chem 268*:20855–20862.

Cleland JL, Wang DI. 1990. Refolding and aggregation of bovine carbonic anhydrase B: Quasi-elastic light scattering analysis. *Biochemistry 29*:11072–11078.

Cover WH, Ryan JP, Bassford PJ, Walsh K, Bollinger J, Randall LL. 1987. Suppression of a signal sequence mutation by an amino acid substitution in the mature portion of the maltose-binding protein. *J Bacteriol 169*:1794–1800.

Debarbouille M, Shuman HA, Silhavy TJ, Schwartz M. 1978. Dominant constitutive mutations in *malT*, the positive regulator gene of the maltose regulon in *Escherichia coli*. *J Mol Biol 124*:359–371.

Edwards MS, Sternberg MJE, Thornton JM. 1987. Structural and sequence patterns in the loops of $\beta\alpha\beta$ units. *Protein Eng 1*:173–181.

Ferenci T, Klotz U. 1978. Affinity chromatographic isolation of the periplasmic maltose-binding protein of *Escherichia coli*. *FEBS Lett 94*:213–217.

Goldberg ME, Rudolph R, Jaenicke R. 1991. A kinetic study of the competition between renaturation and aggregation during the refolding of denaturated-reduced egg white lysosyme. *Biochemistry 30*:2790–2797.

Haase-Pettingell CA, King J. 1988. Formation of aggregates from thermolabile in-vivo folding intermediate in P22 tailspike maturation. *J Biol Chem 263*:4977–4983.

Kraulis PJ. 1991. Molscript: A program to produce both detailed and schematic plots of protein structures. *J Appl Crystallogr 24*:946–950.

Kunkel TA. 1985. Rapid and efficient site-specific mutagenesis without phenotypic selection. *Proc Natl Acad Sci USA 82*:488–492.

Missiakas D, Betton J-M, Raina S. 1996. New components of protein folding in extracytoplasmic compartments of *Escherichia coli* SurA, FkpA and Skp/OmpH. *Mol Microbiol 21*:871–884.

Mitraki A, Betton J-M, Desmadril M, Yon J. 1987. Quasi-irreversibility in the unfolding-refolding transition of phosphoglycerate kinase induced by guanidine hydrochloride. *Eur J Biochem 163*:29–34.

Mitraki A, King J. 1989. Protein folding intermediates and inclusion body formation. *Bio/Technology 7*:690–697.

Nall BT. 1994. Proline isomerization as a rate-limiting step. In: Pain RH, ed. *Protein folding*. New York: Oxford University Press Inc. pp 80–103.

Neu HC, Heppel LA. 1965. The release of enzymes from *Escherichia coli* by osmotic shock and during the formation of spheroplasts. *J Biol Chem 240*:3685–3692.

Nikaido H. 1994. Maltose transport system of *Escherichia coli*: An ABC-type transporter. *FEBS Lett 346*:55–58.

Pace CN. 1986. Determination and analysis of urea and guanidine hydrochloride denaturation curves. *Methods Enzymol 131*:266–280.

Quiocho F. 1991. Atomic structures and function of periplasmic receptors for active transport and chemotaxis. *Curr Opin Struct Biol 1*:922–933.

Sharff AJ, Rodseth LE, Spurlino JC, Quiocho FA. 1992. Crystallographic evidence of a large ligand-induced hinge-twist motion between the two domains of the maltodextrin binding protein involved in active transport and chemotaxis. *Biochemistry 31*:10657–10663.

Shuman HA. 1982. Active transport of maltose in *Escherichia coli* K12. *J Biol Chem 257*:5455–5461.

Sinclair JF, Ziegler MM, Baldwin TO. 1994. Kinetic partitioning during protein folding yields multiple native states. *Nat Struct Biol 1*:320–326.

Song T, Park C. 1995. Effect of folding on the export of ribose-binding protein studied with the genetically isolated suppressors for the signal sequence mutation. *J Mol Biol 253*:304–312.

Speed MA, Wang DIC, King J. 1995. Multimeric intermediates in the pathway to the aggregated inclusion body state for P22 tailspike polypeptide chains. *Protein Sci 4*:900–908.

Spurlino JC, Lu GY, Quiocho FA. 1991. The 2.3-Å resolution structure of the maltose- or maltodextrin-binding protein, a primary receptor of bacterial active transport and chemotaxis. *J Biol Chem 266*:5202–5219.

Wetzel R. 1994. Mutations and off-pathway aggregation of proteins. *Trends Biotechnol 12*:193–198.

Wickner W, Leonard MR. 1996. *Escherichia coli* preprotein translocase. *J Biol Chem 271*:29514–29516.